HELIOS-2: Benchmarking Against Hexagonal Lattices

Teodosi Simeonov[a] and Charles Wemple[b]

[a] *Studsvik Scandpower, GmbH., Hamburg,Germany*
[b] *Studsvik Scandpower, Inc., Idaho Falls, ID, USA*

ABSTRACT

The critical experiments performed at the Hungarian ZR-6 reactor and experiments performed at General Purpose P (GPP) critical facility at RRC "Kurchatov Institute" are used to benchmark HELIOS-2, as part of its ongoing validation and verification activities. The comparisons presented in this paper are based on, ZR6-VVER-EXP-001, Vol. 1 (2007), LEU-COMP-THERM-015, Vol. 4 (2005), and LEU-COMP-THERM-061, Vol. 4 (2002).

On ZR-6, single cell, macro cell, and 2D calculations on selected experiments, regular and perturbed, are made. In the 2D calculations, the radial leakage is treated by including the reflector in the calculations, representing only axial leakage by a measured axial buckling. k_{eff} and RMS reaction rates comparisons are presented.

On GPP critical facility, the entire experiment is modelled as 2D. Comparisons of k_{eff} and fission rates are presented and the effect of the axial buckling on k_{eff} is investigated.

1. INTRODUCTION

HELIOS-2 (Wemple, et al.), is a 2D transport theory program for fuel burnup and gamma-flux calculation. It solves the neutron and gamma transport equations in a general, two-dimensional geometry bounded by a polygon of straight lines. The surrounding medium is described in terms of user-provided boundary conditions.

The system to be calculated may be subdivided into a large number of 'flat flux' regions or space mesh, to support the numerical solution. Material properties may be assigned freely to any mesh. The geometric description of the system is user input controlled, thus almost any fuel cell, fuel assembly, or larger areas of a reactor core may be described. Typical applications include BWR, PWR, VVER, CANDU, RBMK, AGR, MAGNOX, and various test reactor fuel assemblies or larger core regions.

To find the neutron and gamma fluxes, the energy range is discretized into energy groups which are coupled by fission and up-and-down scattering sources. Per energy group, the neutron and gamma transport in general 2D geometry is solved by partitioning the system into space elements, e.g., pin cells, inside which first-flight probabilities are used. These elements are coupled by currents which can have various angular discretizations. It is up to the User to choose the space elements and the angular current discretization.

As an alternative to the collision probabilities method, a method of characteristics (MOC) is available solver has been added to the transport solver module. The MOC solution has been implemented both in the current coupled form (CCCM) and in the uncoupled (k=0) form (the so-called "long characteristics"). Because of reduced memory requirements, the "long characteristics" solution offers improved computational performance from the uncoupled collision probabilities solution and, therefore, the potential for modeling larger, more complex geometries. The MOC has been applied everywhere in this study.

The HELIOS-2 neutron data library is based on ENDF/B-VII R0 evaluated data files (Chadwick, et al., 2006), the most comprehensive evaluations available. The main cross section processing was performed using the NJOY code (MacFarlane and Muir, 1994), version 99.161. Several modifications were made to this code, including the addition of a module that uses NJOY-generated data to build the resonance integral data required for the HELIOS library format. The auxiliary code, HEBE, was used to assemble the processed isotope cross sections and resonance integral data into the final library. The new library contains neutron data for 303 materials, including 121 fission products and 40 actinides, with 80 resonance materials. Photon cross section data are available for 301 materials. The base nuclear data library uses 177 neutron groups and 48 photon groups; a production library with 49 neutron groups and 18 photon groups is also being developed.

In this paper, HELIOS-2 is compared to critical experiments performed at the Hungarian ZR-6 reactor. The data used hereafter is compiled in "The VVER EXPERIMENTS: REGULAR AND PERTURBED HEXAGONAL LETTICES OF LOW-ENRICHED uo2 FUEL RODS IN LIGHT WATER", ZR6-VVER-EXP-001, Revision 0, March 31, 2007, and LEU-COMP-THERM-015, Revision 3, September 30, 2005.

Calculations on single pin-cells, macro cells and 2D calculations on full experimental configurations have been performed. The single cell cases are discussed in Section 2. In the pincell cases, the radial and axial leakage is represented by a measured material buckling, and integral quantities, k_{eff} and δ^{28} (the ratio of the total fission rate of U238 to that of U235) are compared. For macro cells, presented in Section 3, and 2D full configurations, presented in section 4, fission rate comparisons are also shown. Comparisons to other codes results are presented as well. Examples of typical HELIOS outputs processed by ZENITH are shown in the appendix.

2. TIC SINGLE PIN-CELL

Twenty-five single cell cases (also called asymptotic cases), as described in LEU-COMP-THERM-015, Table 16, have been studied. Basic, more or less standard for VVER, space subdivision in the coolant is applied for cells with 11 and 12.7mm pin pitch, while a finer subdivision was found necessary for cells with 15 and 19.05mm pitch. An example is provided in Figure 6 in the Appendix.

Table 1 shows the obtained k_{eff} values and comparison with the results from the 3D nodal code KARATE, where available. Table 2 presents results grouped per lattice type and measurement conditions, while Table 2a shows the effect of applying some technological uncertainties directly to the model in HELIOS-2.

Table 1. Single pin cell criticals.

N	Lattice ID	Temp. [C]	B_m^2 [m^{-2}]	k_{eff} HELIOS	k_{eff} KARATE	Δk_{eff} HELIOS [pcm]	Δk_{eff} KARATE [pcm]
1	12.7/3.6/0	21	100.61	1.00797	1.0082	797	820
2	12.7/3.6/0	80	96.55	1.00438	1.0022	438	220
3	12.7/3.6/0	130	90.27	1.00327	0.9998	327	-20
4	12.7/3.6/4.0	21	74.16	1.01361		1361	
5	12.7/3.6/4.0	80	72.07	1.00928		928	
6	12.7/3.6/4.0	130	67.63	1.00962		962	
7	12.7/3.6/5.8	21	64.95	1.01076	1.0054	1076	540
8	12.7/3.6/5.8	80	61.69	1.01258	1.0059	1258	590
9	12.7/3.6/5.8	130	59.02	1.00978	1.0019	978	190
10	12.7/3.6/7.2	21	56.54	1.01400		1400	
11	12.7/1.6/0.0	21	50.54	1.00197	0.9893	197	-1070
12	12.7/1.6/1.85	21	33.32	1.00003		3	
13	12.7/4.4/0.0	21	112.58	1.00265	1.0032	265	320
14	12.7/4.4/0.64	21	106.60	1.00954	1.0082	954	820
15	12.7/4.4/7.20	21	69.03	1.02078		2078	
16	11.0/3.6/0.0	21	66.01	0.99919	0.9940	-81	-600
17	11.0/3.6/0.0	80	64.02	0.99166	0.9859	-834	-1410
18	11.0/3.6/0.0	130	59.76	0.98894	0.9830	-1106	-1700
19	11.0/3.6/1.0	21	62.14	1.00388	0.9981	388	-190
20	11.0/3.6/1.41	21	61.70	1.00138		138	
21	15.0/3.6/0.0	21	120.36	1.00879	1.0112	879	1120
22	15.0/3.6/4.0	21	70.25	1.01748	1.0134	1748	1340
23	15.0/4.4/0.0	21	136.80	1.00257	1.0054	257	540
24	15.0/1.6/0.0	21	48.90	1.01122	0.9998	1122	-20
25	19.05/3.6/0.0	21	108.20	1.01235		1235	

HELIOS: Average value: 1.00510 Standard deviation: 0.00727 (17 values)
KARATE: Average value: 1.00088 Standard deviation: 0.00859

It can be seen that HELIOS-2 has difficulties reproducing some of the benchmark criticalities, in particular some lattices with relatively higher Boron concentration and lattices with 11mm pitch without Boron. Table 2 gives an overview of lattices with similar properties. The large deviations from Table 1 can also be found here, grouped by lattices properties.

Table.2 HELIOS-2 eigenvalue statistics per lattice type.

Lattice type	Number	k_{eff} Average	Standard deviation [pcm]
1.10 cm pitch	5	0.99701	642
1.27 cm pitch	15	1.00868	552
1.50 cm pitch	4	1.01002	617
1.905cm pitch	1	1.01235	0
1.6wt% enriched	3	1.00441	598
3.6wt% enriched	18	1.00661	760
4.4wt% enriched	4	1.00889	858
Without boron	12	1.00291	712
Dissolved boron	13	1.01021	592
20 centigrades	17	1.00813	641
80 centigrades	4	1.00448	918
130 centigrades	4	1.00290	979
All 25	25	1.00671	739

Based on the analyses of the effect of the technological uncertainties made in the benchmark specification, an attempt to explain those deviations is presented in Table 2a. The results are obtained by directly applying, in the HELIOS-2 model, some technological uncertainties from the benchmark specification. The following uncertainties have been applied:

-average Buckling uncertainties;
-outer cladding radius 0.0025cm;
-H3BO3 concentration 0.5%.

The enrichment uncertainty has not been used in this study, although it is said to have the largest effect, because of its stochastic nature.

Table.2a Per lattice type statistics with applied uncertainties.

Lattice type	Number	k_{eff} Average	Standard deviation [pcm]
1.10 cm pitch	5	1.00259	281
1.27 cm pitch	15	1.00340	312
1.50 cm pitch	4	1.00515	450
1.905cm pitch	1	1.00784	-
1.6wt% enriched	3	1.00558	327
3.6wt% enriched	18	1.00377	279
4.4wt% enriched	4	1.00194	532
Without boron	12	1.00268	380
Dissolved boron	13	1.00463	257
20 centigrades	17	1.00472	331
80 centigrades	4	1.00233	184
130 centigrades	4	1.00070	229
All 25	25	1.00369	330

In Table 2a is shown, that within the range of uncertainty k_{eff} might become more stable, within a standard deviation of 330pcm. This would give more confidence in the overall results. With an average k_{eff} of 1.00369, HELIOS-2 tends to over-estimate the pin cells.

Table 3 shows comparisons between the available measured δ^{28}, the ratio of the total fission rate of U-238 to that of U-235, and the values calculated by HELIOS-2.

Table 3. Measured and calculated δ^{28} values.

Lattice ID	Measured	Calculated	RMS difference [%] (all values)
12.7/1.6/0.0	0.0667 ± 0.0039	0.0672	
12.7/1.6/1.85	0.0673 ± 0.0039	0.0698	
12.7/3.6/0	0.0543 ± 0.0013	0.0594*	6.02**
12.7/3.6/4	0.0671 ± 0.0028	0.0626*	
12.7/3.6/7.2	0.0671 ± 0.0021	0.0652	
12.7/4.4/0.0	0.0557 ± 0.0014	0.0583	
12.7/4.4/0.64	0.0578 ± 0.0014	0.0586	$RMS = \sqrt{\frac{1}{N}\sum\left(\frac{calc}{meas}-1\right)^2}$
12.7/4.4/7.20	0.0656 ± 0.0016	0.0627	
11.0/3.6/0.0	0.0853 ± 0.0027	0.0894	
11.0/3.6/1.41	0.0819 ± 0.0029	0.0916*	

**Remark: The measurement errors are not accounted for.

The relatively big RMS difference is an open question, although more than half of it is due to the three lattices marked with *.

3. TIC MACRO CELLS CALCULATIONS

The results of so called macro cells are presented in Table 4. With the exception of the first two cases, the results follow what has been observed for the single pin cell criticals. Excluding the two lattices marked with (*), the average k_{eff} is 1.00283± 0.00350 and an average fission rate RMS below 0.3% are quite good.

Table 4. Macro cell criticals.

Lattice ID	Temp. [C]	B_m^2 [m^{-2}]	k_{eff}	RMS fission rates [%]
12.7/3.6/0.00 E3	21	107.38	*1.0113**	0.3
12.7/3.6/0.00 C5	21	70.56	1.0067	-
12.7/3.6/0.00 G5	21	40.62	*1.0273**	0.2
12.7/3.6/0.00 E7	130	90.19	1.0048	0.4
12.7/3.6/0.00 F7	21	78.29	1.0025	0.3
12.7/3.6/0.00 G7	21	73.11	1.0055	0.3
12.7/3.6/0.00 G7	130	62.75	1.0028	0.3
11.0/3.6/0.00 E7	21	67.29	1.0011	0.3
11.0/3.6/0.00 E3	21	83.47	0.9961	0.1

The k_{eff} overestimation of about 2.7% for macro cell "12.7/3.6/0.00 G5" is difficult to be explained only in terms of the calculations. Similar systems like "12.7/3.6/0.00 C5" and "12.7/3.6/0.00 G7" behave consistently and the 2D configuration of the same G5 type, 242/242, shows an excellent agreement with the measurement.

4. TIC 2D CALCULATIONS ON CRITICAL EXPERIMENTS

Altogether, 69 "regular" and 63 "perturbed" configurations, from LEU-COMP-THERM-015 Tables 12a and 12b, have been studied. For the 2D configurations presented here, fission rates comparisons are also shown.

The flexibility in describing the geometry in HELIOS-2 offers many possibilities for optimal balance between the best estimate and the computer efficiency, limited in the past by the memory requirements of the collision probabilities solver, which increases quadratically with the number of regions used in the system. The introduction of the method of characteristics, MOC, as an alternative solver in HELIOS-2, eliminates this limitation and offers a possibility to obtain an exact solution for rather large systems. An example for such a system is provided in Figure 9 in the Appendix.

The 2D systems are based on the principle core maps, where the radial leakage is modelled explicitly by including a reflector region about twice the size of the radial extrapolation length, with the axial leakage represented by the measured axial buckling. The spectrum associated with the input buckling is used for the output.

In Table 5, results for a set of 2D configurations are presented: k_{eff}, RMS fission rates, and k_{eff} calculated by the code KENO-Va with the 123-group GAM-THERMOS Library. In lattice "245.244", the original axial buckling 42.24m^{-2} has been replaced by a value of TIC, Vol 1 (1995) due to a significant under-estimation of k_{eff} (k_{eff} ($B_{ax=42.24}$)= 0.97579). Selected maps of fission rates differences are provided in the Appendix, Figures 10-16.

Table 5. 2D configurations – k_{eff} and fission rates

Lattice ID	Pitch [mm]	Enrichment [wt%]	H_3BO_3 [g/l]	B_z^2 [m^{-2}]	k_{eff}	KENOVa	RMS diff. fission rate [%]
Regular configurations							
39.39	11.00	3.6	0.00	8.91	1.00513	0.98820	1.5
40.40	11.00	3.6	0.00	12.79	1.00634	0.97940	2.6
41.41	11.00	3.6	0.00	6.83	1.00691	0.98330	2.0
42.40	11.00	3.6	1.41	7.30	0.99863	0.98520	1.4
154.154	12.70	3.6	0.00	18.01	1.00210	0.98830	2.6
29.29	12.70	3.6	4.00	25.75	1.00398	0.99830	1.6
163.161	12.70	3.6	5.79	14.93	1.00578	0.99360	1.3
38.38	12.70	3.6	7.18	8.03	1.00650	1.00000	1.4
110.110	12.70	4.4	0.00	13.08	1.00354	0.98850	2.2
111.110	12.70	4.4	0.64	6.42	1.00726	0.99030	2.0
112.112	12.70	3.6/4.4	7.18	13.48	1.00605	0.99830	1.3
				Average	1.00475	0.99031	1.8
				Std.Dev.	0.00257		
Perturbed configurations							
57.57	12.70	3.6	0.00	20.03	1.00110	0.99380	1.6
58.57	12.70	3.6	0.00	49.75	0.99837	0.99300	1.2
101.100	12.70	3.6	0.00	64.59	0.99902	0.99990	1.9
113.113	12.70	1.6/3.6/4.4	5.49	11.50	1.00017	0.98400	1.2
147.138	12.70	3.6	1.80	34.53	1.00262	0.99630	1.7
245.244	12.70	3.6	0.00	40.88*	0.99510	0.99050	1.2
156.155	12.70	3.6	0.00	22.21	1.00313	0.99580	1.9
176.176	12.70	3.6	0.00	24.66	1.00233	0.99460	1.8
241.241	12.70	3.6	0.00	17.05	1.00584	0.99320	3.6
190.190	11.00	3.6	0.00	19.43	0.99824	0.98930	9.2**
189.189	11.00	3.6	0.00	8.50	1.00871	0.98540	1.4
				Average	1.00133	0.99235	1.75
				Std.Dev.	0.00380		

* - the original buckling is replaced by a value from an old TIC evaluation;
** - value excluded from the average.

The 2D configurations are divided into two parts: regular and perturbed. For the presented cases, HELIOS-2 shows very consistent results with a relatively small standard deviation. The "regular" k_{eff} values tend to be higher. The RMS errors of the fission rates are also in quite good agreement with the experiment, with an average value of 1.8%.

In Table 6, the "regular" configurations, sorted by type, are compared to other codes results published in the benchmark specification.

Table 6. Regular lattice statistics.

Type	N of cases (HELIOS-2)	HELIOS-2	KENOVa (H.-R.)	KENOVa (27-gr)	KENOVa (123-gr)	KARATE
11.0/3.6	8	1.00652	0.99440	0.98430	0.98420	0.99400
12.0/4.4	1	1.00354	0.99100	0.99270	0.99280	1.00820
12.7/3.6/0	10	1.00182	0.98930	0.99290	0.99030	1.00320
12.7/3.6/4	10	1.00297	0.99450	0.99440	0.99620	-
15.0/4.4/0	8	0.99503	0.99200	0.99740	0.99690	1.00540
15.0/3.6/0	8	0.99183	0.99320	0.99570	0.99700	1.01120
15.0/3.6/4	6	1.00116	1.00190	1.00050	1.00170	1.00140
19.05/3.6/0	11	0.99215	1.00930	1.00200	1.00260	-

Note. The eight configurations based on principal map 204 are not included.

It can be seen that HELIOS-2 returns higher k_{eff} for 11mm and 12.7mm pitch, while under estimating it for the 15mm and 19.05mm lattices. This might be partly explained with the mesh chosen for this comparison, being the same for all lattices: 18 regions in the coolant and two in the fuel, which may be insufficient for the configurations with larger pin pitch. In general, it seems that HELIOS-2 predicts the integral and local results very well. However, a closer look into the "regular" lattices would show this from a different perspective.

The average k_{eff} for 69 configurations is very good (0.99964), but the standard deviation (0.00679) is something that one should not easily neglect. Figure 1 shows the regular results grouped by principal map used in their compilation at constant boron concentration via the axial buckling.

Figure 1. Regular delta k_{eff} by configuration type versus the axial buckling.

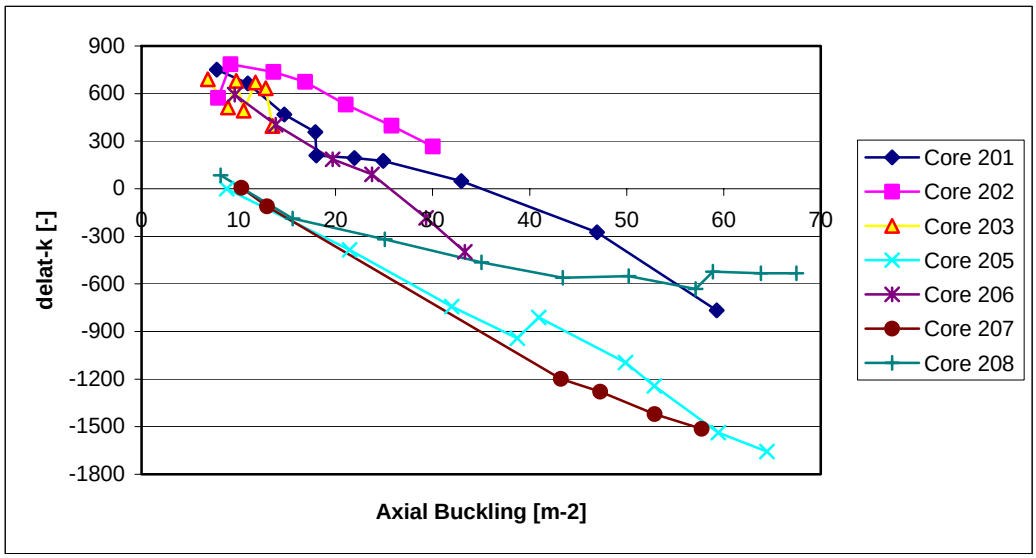

The trend on Figure 1 is quite clear. No reasonable explanation from the analyses point of view has been found for this more or less systematic behavior. Such a trend cannot be found if similar figure is produced for the "perturbed" lattices, as can be seen in Figure 2, which suggests that the methods used to calculate the axial bucklings should be given additional examination. The k_{eff} for 63 perturbed configurations is 1.00088±0.00365.

Figure 2. Perturbed delta k_{eff} by configuration type versus the axial buckling.

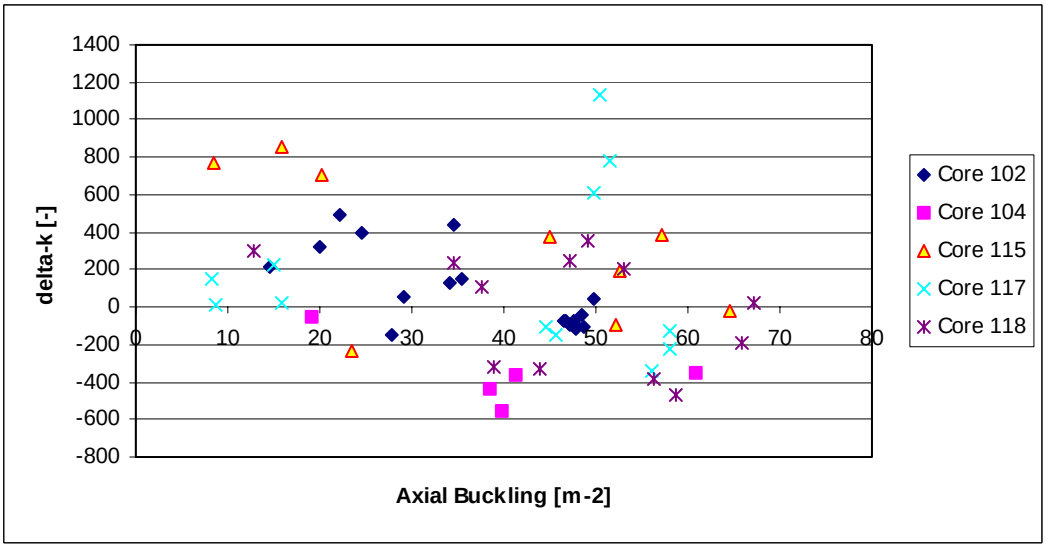

5. GPP CALCULATIONS ON CRITICAL EXPERIMENTS

The GPP VVER benchmark, described in LEU-COMP-THERM-061, describes a series of ten critical measurements for hexagonal lattices using VVER-type materials and lattice configurations. Two series of measurements were performed: the first to define reactivity worths for various types of absorber rods (eight configurations); the second to define the effect of aluminium displacer rods on the core eigenvalue and local fission rates (two configurations). The benchmark specification only defines a 3D configuration, so axial bucklings were derived for these calculations from the measured critical heights. All configurations used a similar pincell lattice. The lattice pitch is 12.7mm, with a 3.7875mm fuel radius and 4.5225mm clad outer radius. The fuel enrichment was fixed at 4.4% U235 by weight. Criticality in the measurements was achieved by variation of the moderator level, which was unborated for the first series and contained approximately 0.5 g/l boric acid for the second series.

In the first series of measurements, four different absorber rod types (B_4C, Hf, Hf tube, and Dy_2O_3) were placed in two different sets of locations in the core (see Figures 3 and 4). In the second series, a ring of Al displacer rods was incorporated into the core in one configuration and replaced by coolant in the second (see Figure 5). Critical moderator heights were between 750mm and 970mm.

Figure 3. Series 1 geometric configuration for absorber rod locations A.

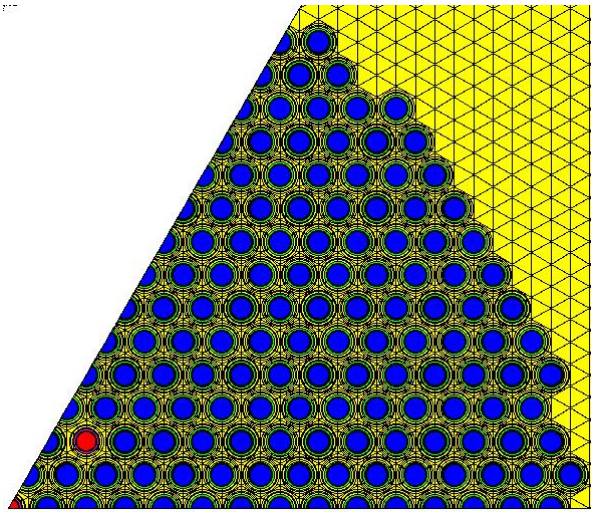

The HELIOS-2 model for the GPP cases used spatial subdivision in both the fuel pin (three radial rings) and the moderator regions (four radial subdivisions, each with 6 azimuthal subdivisions.) The radial reflector, with a thickness of at least 200mm, was included for all configurations. One-sixth core geometry was used for all configurations. All dimensions and material compositions were gleaned from the benchmark specification (LEU-COMP-THERM-061). Axial bucklings were based on the measured critical heights, with extrapolation lengths derived from calculated core-averaged diffusion coefficients. Note that the reflector regions were explicitly excluded from the calculation of the extrapolation lengths. The benchmark eigenvalue, including uncertainties, was defined as 1.0005±0.0023. Core eigenvalues were calculated for each of the ten critical configurations in the benchmark specification; in addition, fission rates were also calculated for 18 pins in the Al displacer rod configuration (see Figure 5a). All calculations used the MOC solver in HELIOS-2.

Figure 4. Series 1 geometric configuration for absorber rod locations B.

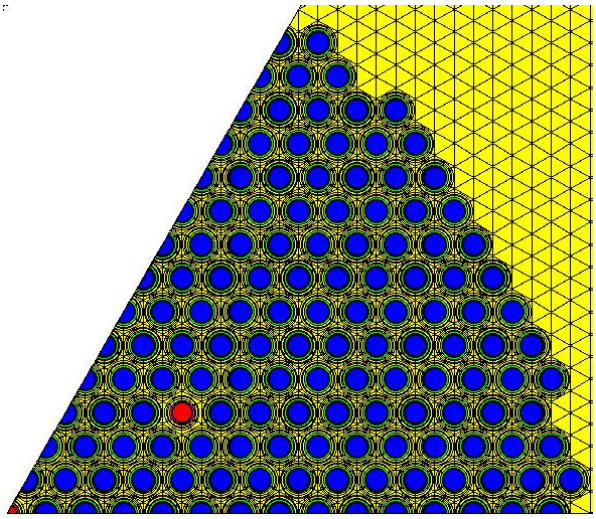

Figure 5. Series 2 geometric configuration.

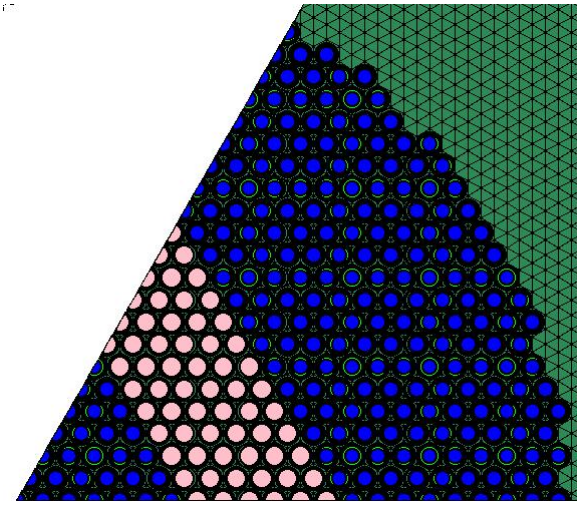

Figure 5a. Location of fission rate measurements in Case 9 (series 2, case 1).

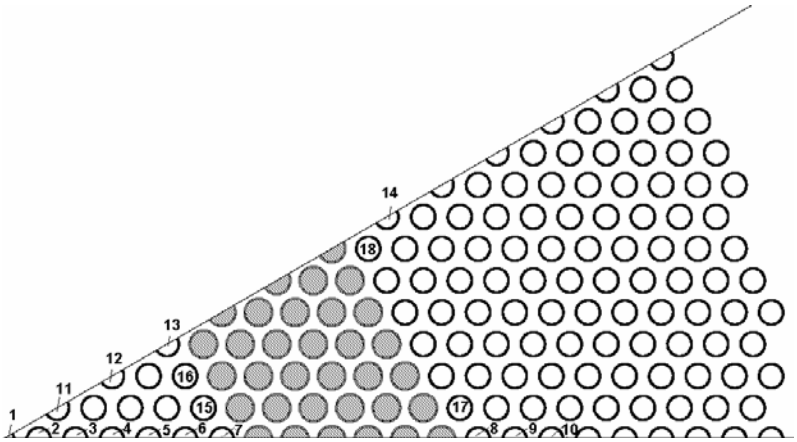

The results of the core eigenvalue calculations are shown in Table 7 for various values of the current coupling parameter, k. The values of k used denote the number of azimuthal angular sectors used to define the current at interfaces between space elements; k=0 corresponds to "perfect coupling", where no approximation is made for the angular dependence of the interface currents; this is the so-called "long characteristics" mode.

Table 7. Core k_{eff} for various values of the coupling coefficient, k.

Case	Buckling (m^{-2})	k=3	k=4	k=7	k=8	k=0
B_4C, conf. A	10.58	1.04268	1.00498	1.00456	0.99986	0.99182
B_4C, conf. B	10.65	1.04124	1.00360	1.00305	0.99840	0.98921
Hf, conf. A	11.66	1.04394	1.00633	1.00584	1.00119	0.99242
Hf, conf. B	12.06	1.04222	1.00462	1.00412	0.99942	0.99036
Hf tube, conf. A	15.31	1.03982	1.00234	1.00176	0.99719	0.98957
Hf tube, conf. B	16.36	1.03691	0.99963	0.99895	0.99437	0.98763
Dy_2O_3, conf. A	16.51	1.03591	0.99855	0.99794	0.99339	0.98497
Dy_2O_3, conf. B	17.36	1.03374	0.99644	0.99578	0.99126	0.98305
Displacer rods	30.97	1.03543	1.01400	1.01337	1.01073	---
No displacers	15.09	1.03432	1.00995	1.01037	1.00719	---

The results in Table 7 demonstrate the effects of increasing the angular fidelity of the space element coupling. The steady drop in k_{eff} with increasing angular fidelity for the absorber rod cases demonstrates the necessity of accurate angular modeling in calculations with strong absorbers.

Table 8. Core k_{eff} for various values of the axial buckling.

Buckling (m^{-2})	Lower energy (keV)	k_{eff}
10.58	---	1.00498
10.30	0.0	1.00585
9.59	1.0	1.00833
9.26	100.0	1.00949
8.65	1000.0	1.01162

Table 8 shows the effect of varying axial buckling on one configuration (B_4C, conf. A) for k=4. In this table, the various axial bucklings correspond to extrapolation lengths calculated with core-averaged transport cross sections (σ_{tr}) for several different energy ranges; the lower energy bounds for each case are given in the table. Selection of an appropriate extrapolation length can have a significant effect on k_{eff} – in this case, a change of nearly 700pcm. Application of this buckling to the k=0 results in Table 7 would greatly improve the calculated k_{eff}, bringing the values close to 1.0; similar improvement would be expected from the other configurations.

Table 9 shows the comparison of measured and calculated fission rates for the 18 locations in the Al displacer rod case, as shown in Figure 5a. The measurement errors range from 1-8%; in this light, the calculated fission rates, with an RMS error of just over 3%, demonstrate excellent agreement.

Table 9. Comparison of measured and calculated relative fission rates for series 2, case 1.

Location	Measured	Calculated	% Difference
1	0.769	0.761	1.019
2	0.767	0.763	0.506
3	0.758	0.774	-2.073
4	0.796	0.807	-1.334
5	0.919	0.896	2.509
6	1.096	1.120	-2.183
7	1.622	1.662	-2.451
8	0.867	0.919	-5.957
9	0.671	0.663	1.183
10	0.597	0.563	5.639
11	0.754	0.769	-2.047
12	0.887	0.847	4.512
13	1.409	1.389	1.450
14	0.854	0.858	-0.442
15	1.517	1.456	3.997
16	1.453	1.400	3.617
17	1.035	1.087	-5.069
18	1.228	1.266	-3.069
RMS	---	---	3.322

6. SUMMARY AND CONCLUSIONS

For many years, the so called TIC VVER benchmark has been a very good tool for 2D and 3D codes validation, despite being rather computationally intensive from the point of view of the 2D neutron transport codes. HELIOS was originally benchmarked against TIC in 1996. In this paper, HELIOS-2 has been used to study the 2007 evaluation of TIC. The new transport solver, MOC, has demonstrated its excellent abilities to calculate TIC's rather large configurations in the "long characteristics" mode.

Single pin cells, macro cells and 2D configurations have been studied and presented in this paper. In general, the agreement with experimental k_{eff} is good. It has been also shown that for the asymptotic cases, HELIOS-2 has shown very good results within the range of the technological uncertainties: k_{eff} = 1.00369±0.00330. However, the δ^{28} RMS difference of 6.0% is considered an open question.

Similar results have been demonstrated for the macro cells and the 2D perturbed configurations with k_{eff}: 1.00283±0.0035 and 1.00088±0.00360. For the regular configurations, although still good if taken as average 0.99964±0.00679, a not well understood tendency of underestimating the critically increasing the equivalent radius has been pointed out.

The ability of HELIOS-2 to calculate the fission rates has been also demonstrated for a few cases of macro cells and 2D configurations. With an average RMS of 1.8%, the 2D fission rates are in very good agreement with the measurements, while the agreement of 0.3% with the macro cells is excellent.

Equally good results, for both eigenvalue and fission rates, also have been demonstrated for the GGP VVER benchmark.

REFERENCES

Wemple C A, H-N.M. Gheorghiu, R.J.J. Stamm'ler, E.A. Villarino (2007) "Recent Advances in the HELIOS-2 Lattice Physics code," International Conference on the Physics of Reactors (PHYSOR-08), Interlaken, Switzerland, 2008.

The VVER Experiments: Regular and Perturbed Hexagonal Lattices of Low-Enriched UO2 Fuel Rods in light Water reactors. NEA/NSC/DOC/(2006)1, ZR6-VVER-EXP-001, Revision 0, March 31,2007, LEU-COMP-THERM-015, Revision 3, September 30, 2005.

Macfarlane R E and Muir D W (1994) "The NJOY Nuclear Data Processing System, Version 91," LA-12740-M, Los Alamos National Laboratory.

Chadwick M B, et al. (2006) "ENDF/B-VII.0: Next Generation Evaluated Nuclear Data Library for Nuclear Science and Technology," *Nuclear Data Sheets* **107**, 2931.

APPENDIX

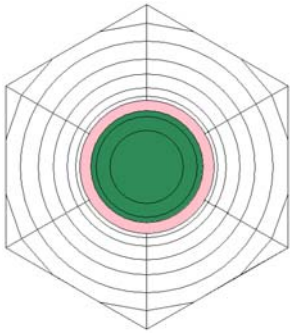

Figure 6. Single pin cell geometry. Pin cell pitch 19.05mm.

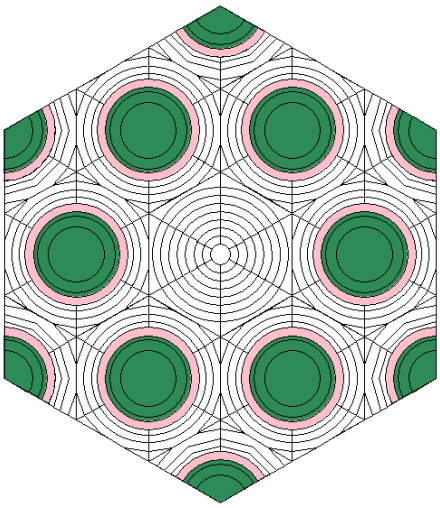

Figure 7. Macro cell type E3 geometry.

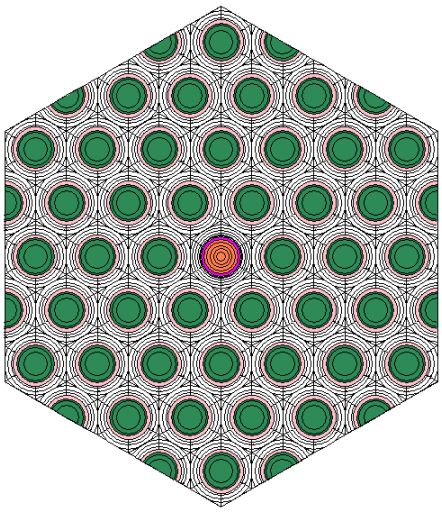

Figure 8. Macro cell type G7 geometry.

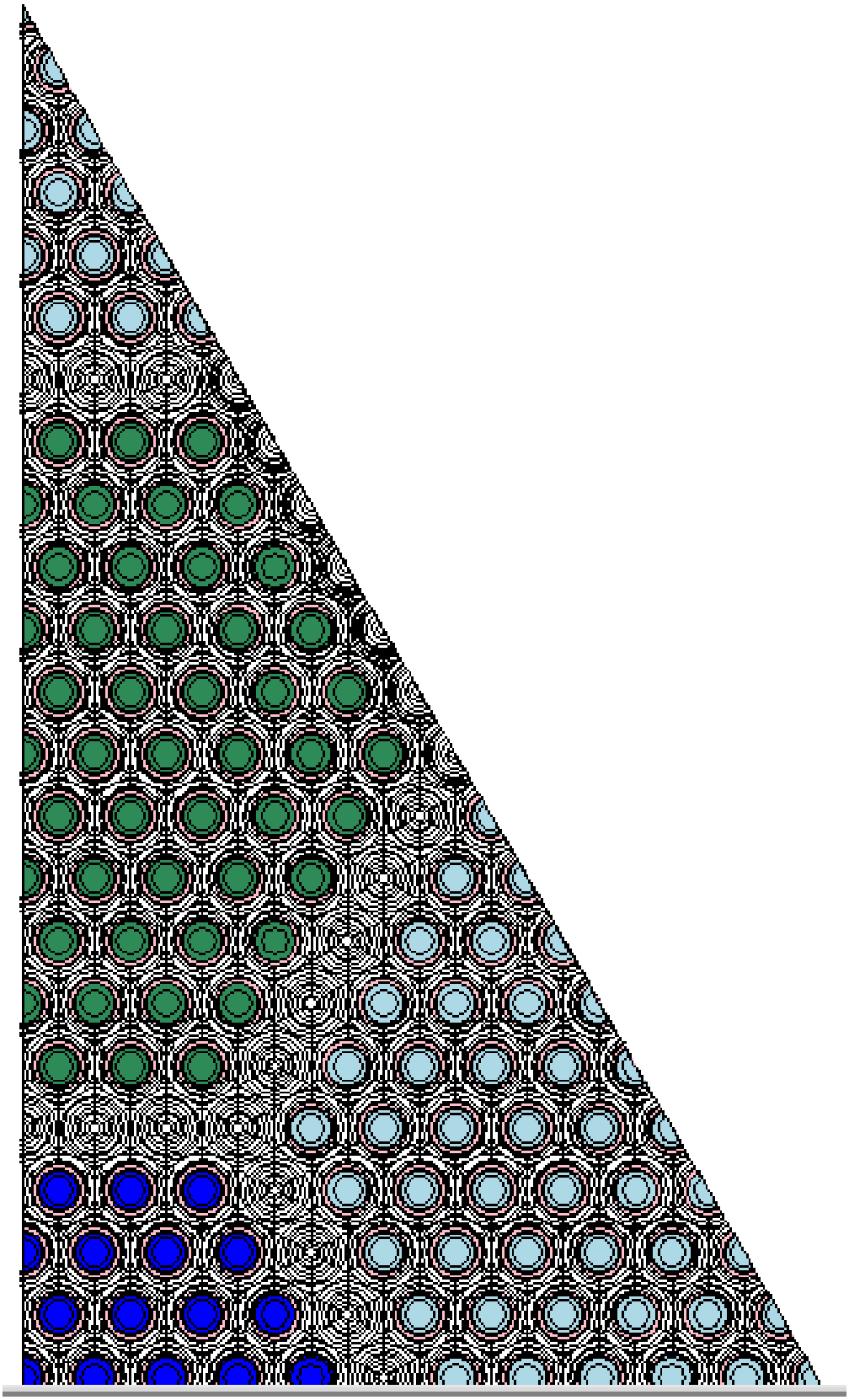

Figure 9. Part of a 2D configuration - TIC case 113/113 (K91)

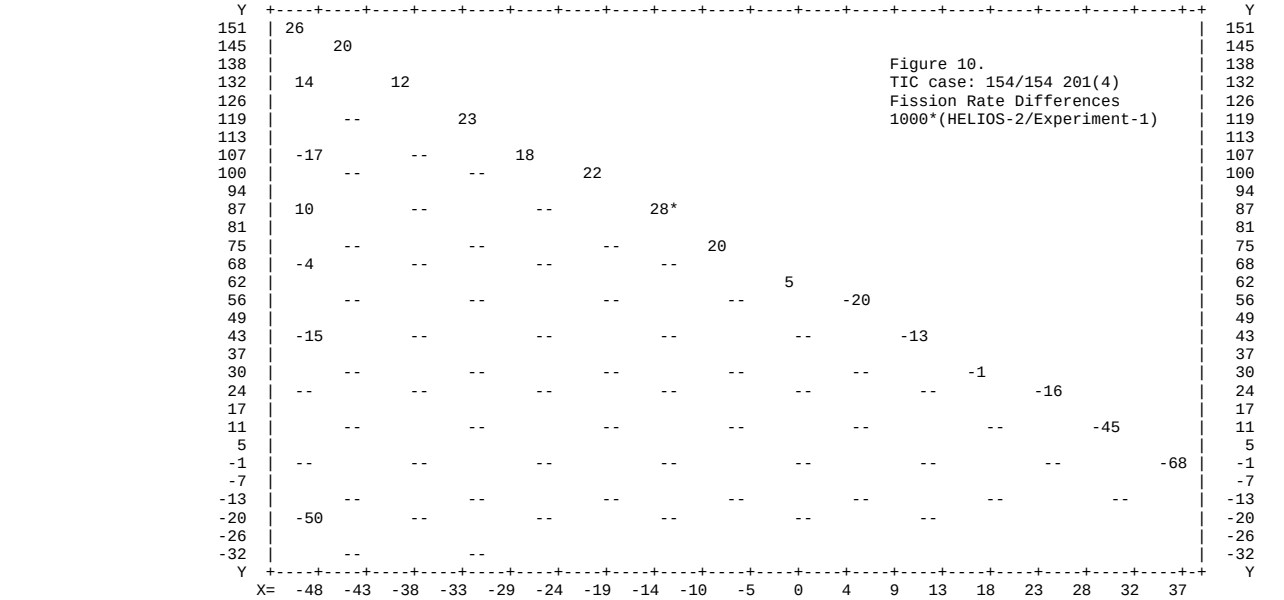
Figure 10.
TIC case: 154/154 201(4)
Fission Rate Differences
1000*(HELIOS-2/Experiment-1)

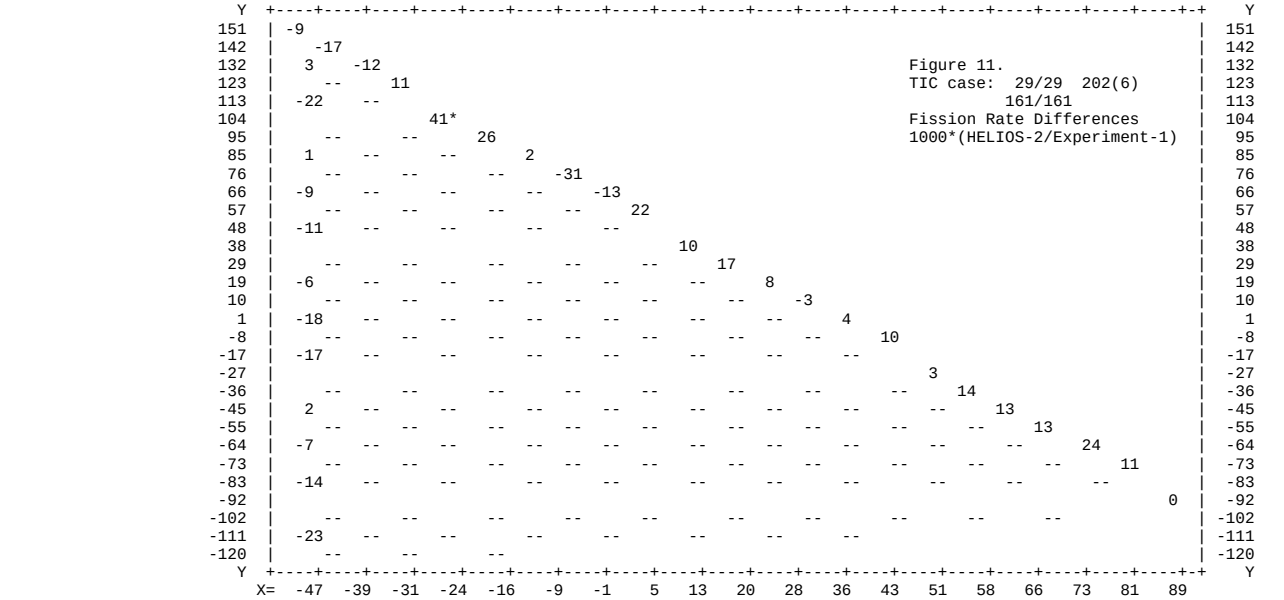
Figure 11.
TIC case: 29/29 202(6)
161/161
Fission Rate Differences
1000*(HELIOS-2/Experiment-1)

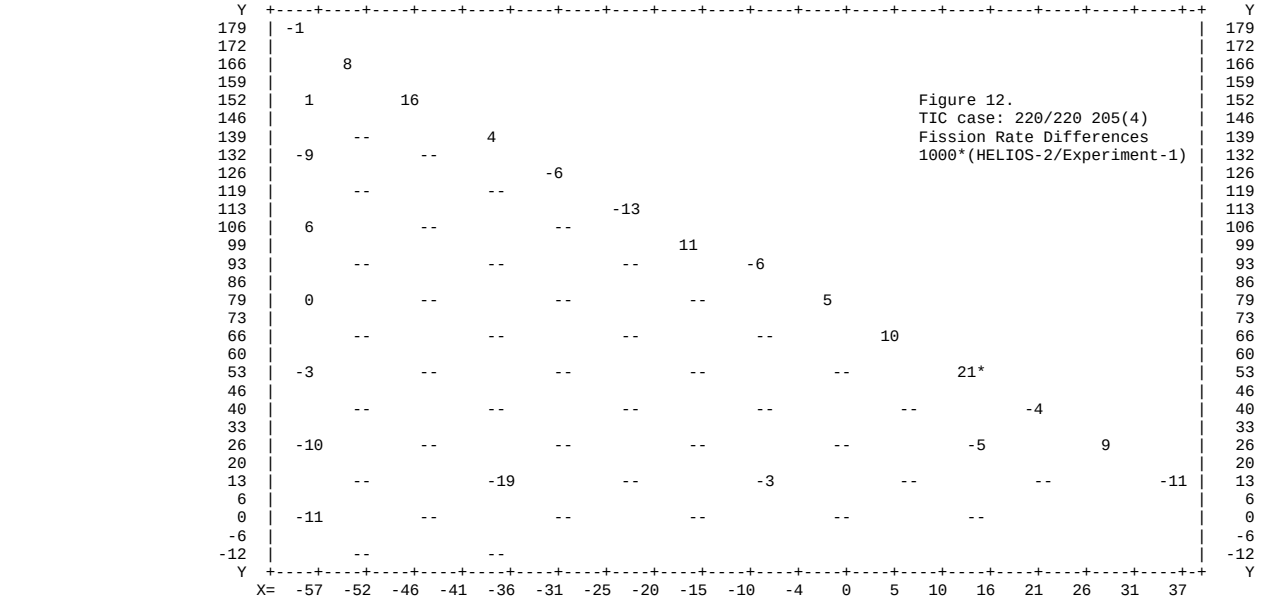
Figure 12.
TIC case: 220/220 205(4)
Fission Rate Differences
1000*(HELIOS-2/Experiment-1)

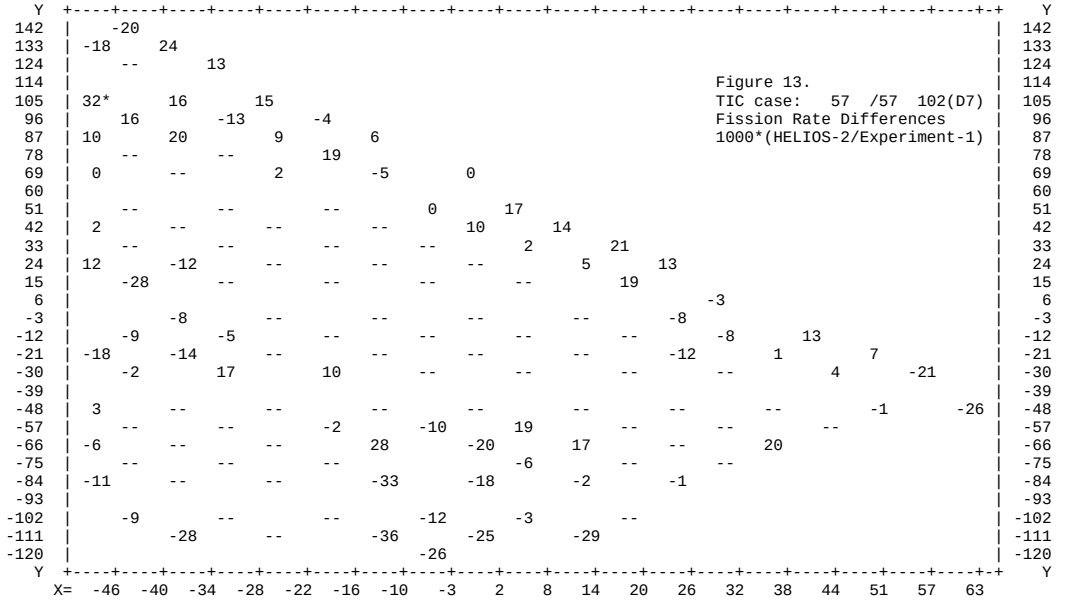
Figure 13.
TIC case: 57 /57 102(D7)
Fission Rate Differences
1000*(HELIOS-2/Experiment-1)
X= -46 -40 -34 -28 -22 -16 -10 -3 2 8 14 20 26 32 38 44 51 57 63
Y 142 133 124 114 105 96 87 78 69 60 51 42 33 24 15 6 -3 -12 -21 -30 -39 -48 -57 -66 -75 -84 -93 -102 -111 -120

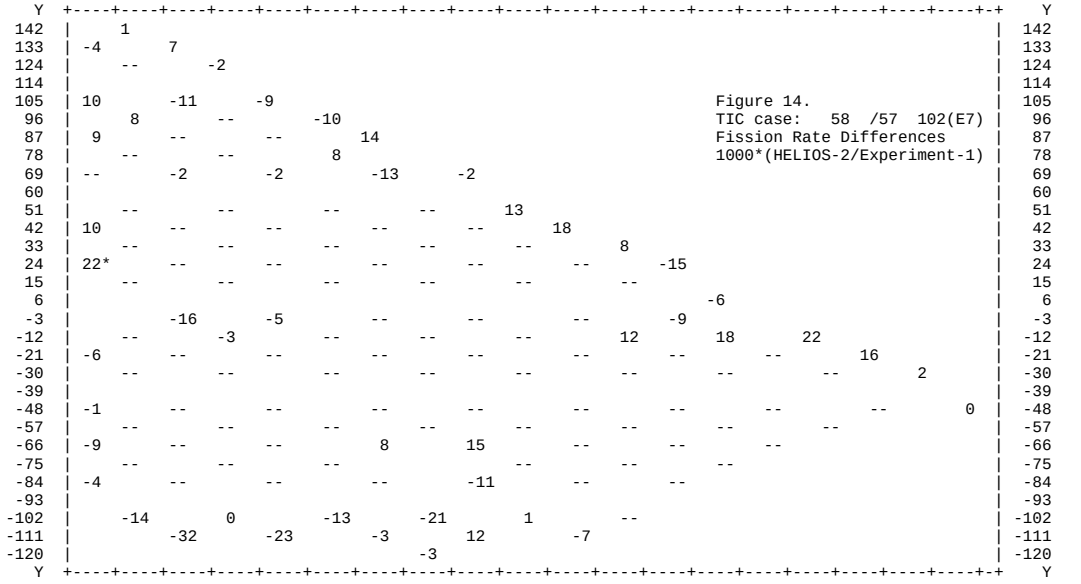
Figure 14.
TIC case: 58 /57 102(E7)
Fission Rate Differences
1000*(HELIOS-2/Experiment-1)
X= -46 -40 -34 -28 -22 -16 -10 -3 2 8 14 20 26 32 38 44 51 57 63
Y 142 133 124 114 105 96 87 78 69 60 51 42 33 24 15 6 -3 -12 -21 -30 -39 -48 -57 -66 -75 -84 -93 -102 -111 -120

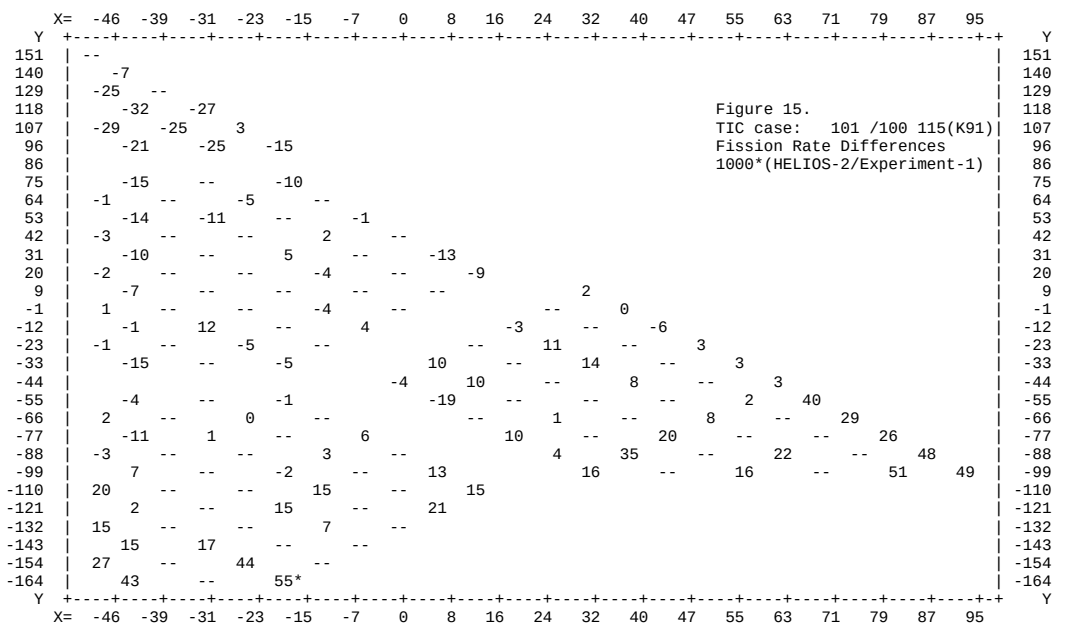
Figure 15.
TIC case: 101 /100 115(K91)
Fission Rate Differences
1000*(HELIOS-2/Experiment-1)
X= -46 -39 -31 -23 -15 -7 0 8 16 24 32 40 47 55 63 71 79 87 95
Y 151 140 129 118 107 96 86 75 64 53 42 31 20 9 -1 -12 -23 -33 -44 -55 -66 -77 -88 -99 -110 -121 -132 -143 -154 -164

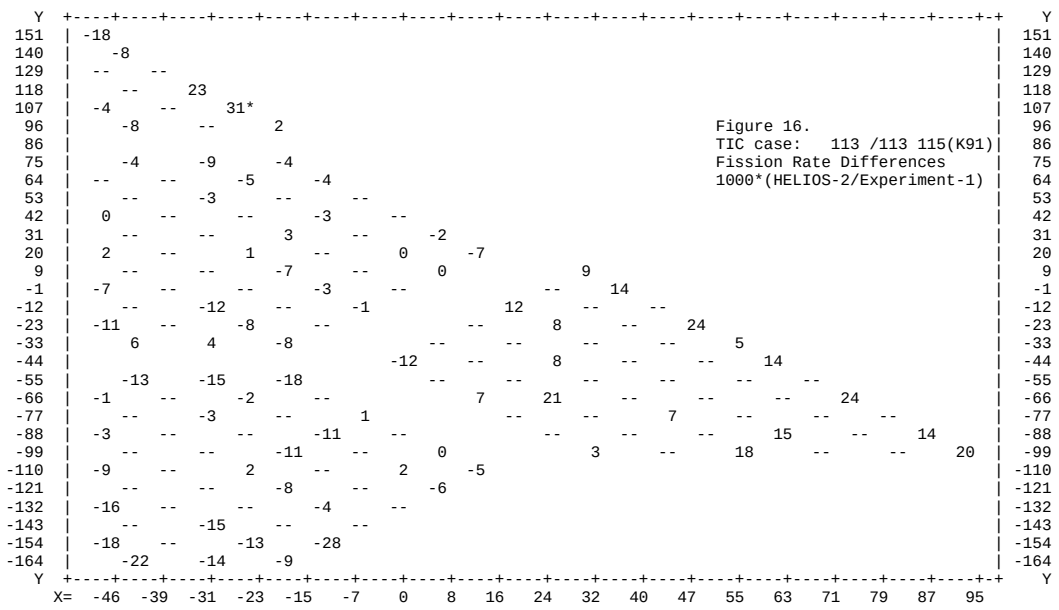
Figure 16.
TIC case: 113 /113 115(K91)
Fission Rate Differences
1000*(HELIOS-2/Experiment-1)
Y
X= -46 -39 -31 -23 -15 -7 0 8 16 24 32 40 47 55 63 71 79 87 95